Observations and Modeling of SST Influence on Surface Winds

Dudley B. Chelton and Qingtao Song

College of Oceanic and Atmospheric Sciences
Oregon State University, Corvallis, OR 97331-5503
chelton@coas.oregonstate.edu, qsong@coas.oregonstate.edu

ABSTRACT

This paper summarizes observational evidence for SST influence on surface winds and the representation of this ocean-atmosphere interaction in atmospheric numerical models. The observed coupling between SST and surface winds is too weak by a factor of 2 or more in global operational forecast models and coupled climate models. From simulations with the Weather Research and Forecasting mesoscale model, it is shown that the primary factors responsible for this underestimation in the global models are: 1) grid resolution; 2) the resolution of the SST boundary condition (and, presumably, the resolution of the ocean component of coupled models); and 3) the dependence of the parameterization of vertical mixing on atmospheric stability. Based on ongoing studies with the operational forecast centers, the third factor is the most challenging to implement.

1. Introduction and Background

Satellite observations of surface winds from QuikSCAT and sea-surface temperature (SST) from the Advanced Microwave Scanning Radiometer (AMSR) have revealed a strong coupling between surface winds and SST in midlatitude regions of strong SST fronts (see reviews by Xie, 2004; Small et al., 2008). This coupling becomes clear after averaging over periods of a month or longer to reduce the effects of synoptic weather variability on surface winds that are unrelated to SST (Fig. 1a). On wavelength scales smaller than about 1000 km, the wind stress magnitude is linearly related to SST (right panels of Fig. 1a) with locally higher winds over warmer water and lower winds over cooler water. Surface wind speed is also linearly related to SST (e.g., O'Neill et al., 2008; see also Figs. 3–5 below). The detailed dynamics for this deceptively simple coupling are complex; all terms in the momentum balance are important (O'Neill et al, 2008). However, a critical factor is the sensitivity of vertical mixing to variations in atmospheric stability. Enhanced vertical mixing over warmer water increases surface winds through downward mixing of momentum. Diminished vertical mixing over cooler water decouples the surface winds from the stronger winds aloft, resulting in decreased surface winds. Nonlinear advection and pressure gradients also play important roles in determining the detailed structure of low-level wind response to SST.

The slope of the linear relation between wind speed or wind stress magnitude and SST (referred to here as the coupling coefficient) computed from spatially high-pass filtered monthly averages varies geographically and temporally (more so for stress magnitude than wind speed); the coupling is generally stronger over the Southern Ocean than over midlatitude SST fronts in the northern hemisphere and is stronger in winter than in summer. These differences are attributable to differences in ambient conditions (primarily the wind speed that is stronger in winter and in the southern hemisphere, but likely also the boundary layer depth and the stability profile within the boundary layer).

The observed SST influence on surface winds is clearly evident in the operational European Centre for Medium-Range Weather Forecasts (ECMWF) model (Chelton, 2005; Maloney and Chelton, 2006; Song et al., 2008), but with coupling coefficients that are only about half of the observed values (right panels of Fig. 1b). Between 9 May 2001 and 31 January 2006, the ECMWF model used NOAA Real-Time Global (RTG) SST analyses as the ocean boundary condition and had a TL511 spectral dynamical core, equivalent to a grid

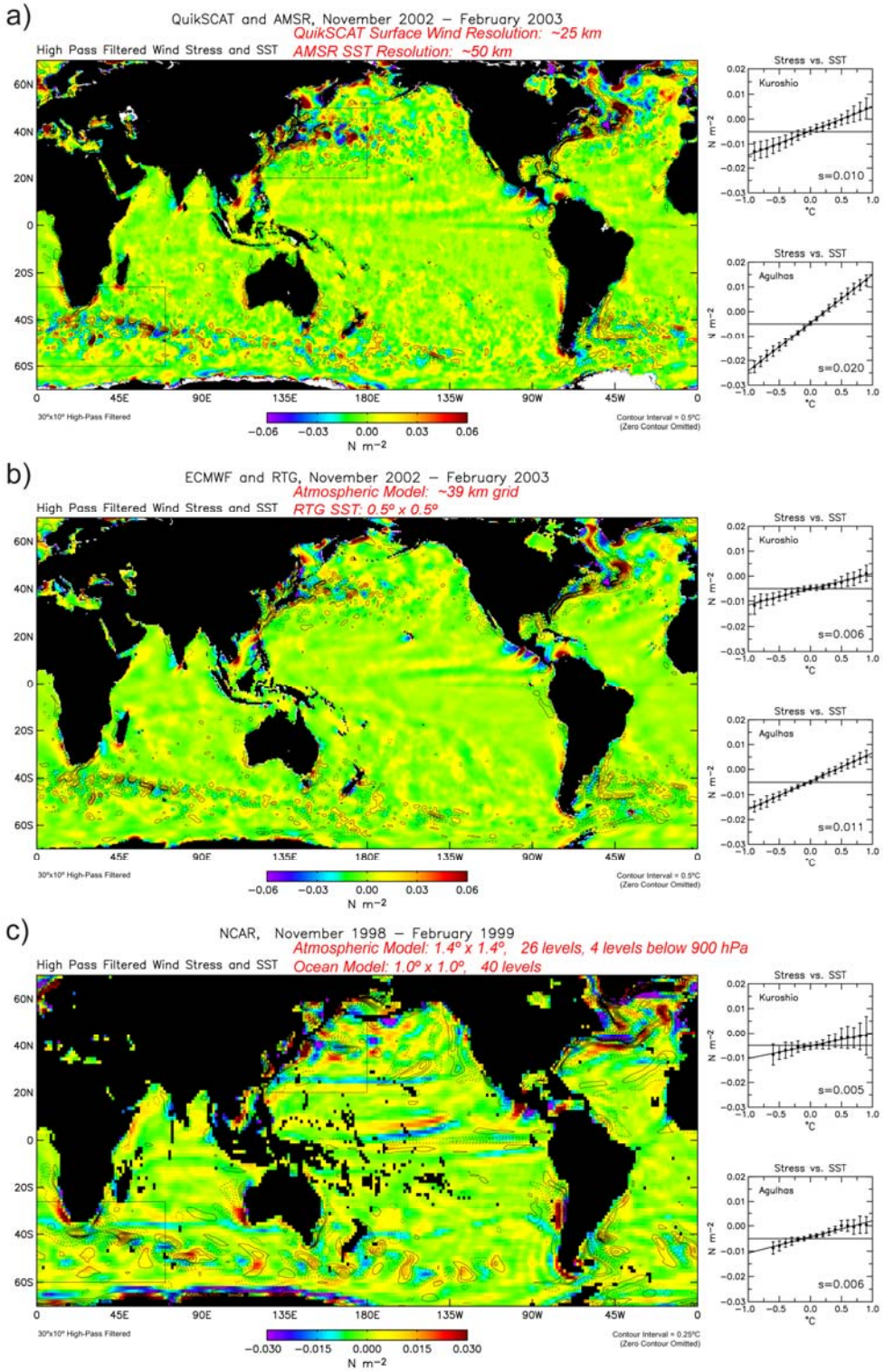

Figure 1 Maps of spatially high-pass filtered wind stress magnitude and SST over 4-month periods November-February from a) satellite observations (QuikSCAT and AMSR); b) the operational ECMWF model with RTG SST; and c) the NCAR CCSM3.0 coupled climate model. The filtering attenuates variability with scales longer than 30° of longitude by 10° of latitude. Note that the contour interval and dynamic range of the color bar in panel c are half those in panels a and b. Note also that the NCAR CCSM3.0 model run is a coupled run without data assimilation and is therefore not intended to represent reality; the map shown is a representative November-February period from the model run. Binned scatter plots of wind stress magnitude dependence on SST constructed from monthly mean fields over 2-year periods are shown on the right for the Kuroshio Extension and Agulhas Return Current regions (top and bottom of each pair of panels). The slopes of the least-squares fit lines through the binned averages are referred to here as the coupling coefficients. (After Maloney and Chelton, 2006.)

resolution of approximately 39 km. (The ECMWF model grid was changed to TL799, corresponding to approximately 25 km grid spacing, on 1 February 2006, and the SST boundary condition was changed from RTG to OSTIA on 30 September 2008.)

The observed SST influence on surface winds is also clearly evident in coupled climate models that have sufficient grid resolution (Maloney and Chelton, 2006). The coupling between SST and wind stress magnitude is shown for the NCAR CCSM 3.0 model in Fig. 1c, which has a 1.4° grid for the atmospheric component of the model and a 1° grid for the oceanic component. The spatial scales of the SST-induced perturbations are much too large, but are nonetheless visually apparent (more consistently over the Southern Ocean than in the northern hemisphere). The coupling coefficients (right panels of Fig. 1c) are comparable to those in the ECMWF model, i.e., smaller than the observed coupling by a factor of 2-3.

The importance of the resolution of the SST boundary condition is readily apparent from examination of the ECMWF model output before and after the 9 May 2001 change of the SST boundary condition from the low-resolution Reynolds SST analyses (Reynolds et al., 2002) to the higher-resolution RTG SST analyses (Thiebaux et al., 2003). Maps of the surface wind field reveal considerably more energetic small-scale structure after changing to the RTG SST analyses (Chelton, 2005; Chelton and Wentz, 2005; Maloney and Chelton, 2006). As shown in the top panel of Fig. 2, there was an abrupt increase in the small-scale variance of ECMWF 10-m wind speeds over SST frontal regions throughout the World Ocean immediately after the 9 May 2001 improvement of the SST boundary condition. The change of the SST boundary condition had no discernable effect on the surface wind speeds over land (bottom panel of Fig. 2). In contrast, the 21 November 2000 change of the ECMWF model from TL319 to TL511 (corresponding to a grid resolution change from about 60 km to about 39 km) resulted in a significant increase in the variance of small-scale surface wind speeds over land (presumably because of the improved representation of mountain topography) but had no discernable effect on wind speeds over the ocean.

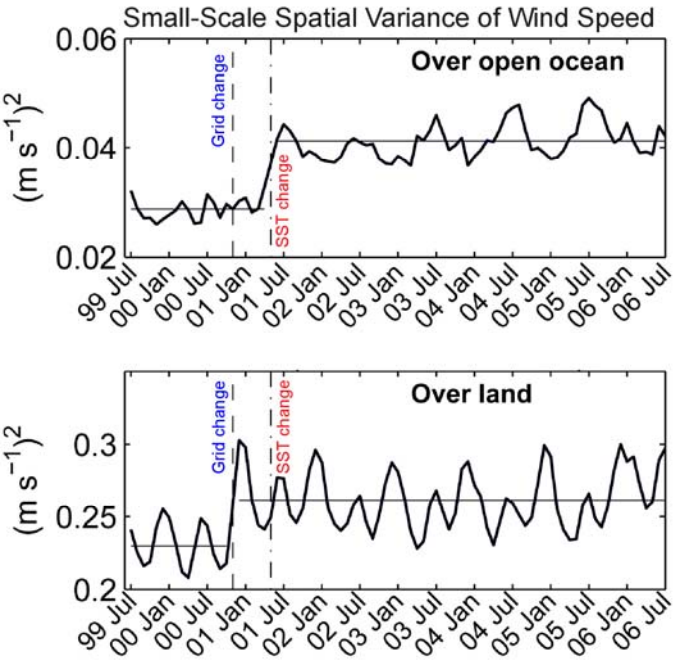

Figure 2 Time series of the spatial standard deviation of 10-m wind speeds in monthly averages from the operational ECMWF model over SST frontal regions of the ocean (top panel) and over continental land masses (bottom panel) (see Song et al., 2008, for details). The vertical dashed lines correspond to times of major changes of the ECMWF model: The grid resolution was changed from TL319 to TL511 (i.e., from about 60 km to about 40 km) on 21 November 2000 and the SST boundary condition was changed from the Reynolds SST analyses to the RTG SST analyses on 9 May 2001. (From Song et al., 2008.)

The coupling coefficients for the NCEP model (not shown here) are very similar to those for the ECMWF model. However, the SST-induced small-scale features in the surface wind field are considerably smoother in the NCEP model (see Figures 13–15 of Chelton and Wentz, 2005) because it continues to use the smooth Reynolds SST analyses as the surface boundary condition.

The reasons for the underestimation of surface wind response to SST in the operational models, and by inference in the coupled climate models, have been investigated by Song et al. (2008) from sensitivity studies conducted with the Weather Research and Forecasting (WRF) mesoscale model. The results of these sensitivity studies are summarized here.

2. Scatterometer Measurements of Surface Winds

The assessment here of the SST influence on surface winds in numerical models is based on comparisons with the coupling deduced from surface winds measured by the QuikSCAT scatterometer. Scatterometers measure surface wind stress. For convenience in a broad range of applications, the measurements are archived as the equivalent neutral stability wind at 10 m, i.e., the 10-m wind that would produce the observed stress if the atmosphere were neutrally stable (Liu and Tang, 1996). The stress at the sea surface measured by a scatterometer is thus related to the equivalent neutral stability wind at 10 m by the bulk formulation with a drag coefficient for neutrally stable conditions, regardless of the actual stability at the time of the scatterometer observation. When compared with buoy winds converted to equivalent neutral stability winds at 10 m as described by Liu and Tang (1996), the accuracy of QuikSCAT winds is essentially the same as that of highly calibrated buoys (Chelton and Freilich, 2005).

Note that the equivalent neutral stability wind speed at 10 m, denoted here as u_{10}^{N}, seldom differs by more than a few tenths of a meter per second from the actual winds at 10 m, denoted as u_{10} (Mears et al., 2001). Because the atmospheric boundary layer is usually slightly unstable over the ocean, u_{10}^{N} is typically about 0.2 ms^{-1} higher than u_{10} (see Fig. 16 of Chelton and Freilich, 2005). As a consequence, the coupling coefficients for u_{10}^{N} are generally 10–15% higher than those inferred from u_{10} (Song et al., 2008).

3. WRF Model Sensitivity Studies

The WRF model simulations conducted by Song et al. (2008) were designed to investigate the sensitivity of surface wind response in the Agulhas Return Current (ARC) region of the South Indian Ocean to a wide range of factors. The ARC region is well suited to such studies because of its isolated location far from continental influence and because of the persistent strong, meandering SST front that is present year-round in this region in association with the eastward flowing Agulhas Return Current.

The WRF model simulations were run for the month of July 2002 in a nested configuration centered on the ARC region with an inner domain of 54ºS to 37ºS and 46ºE to 86ºE and 50 vertical levels. To avoid model drift, the WRF simulations were constrained by outer boundary conditions obtained from the NCEP analyses on a 1º by 1º grid. The model runs included a variety of grid resolutions, SST boundary conditions, and horizontal and vertical mixing parameterizations. The SST boundary condition for each model run was specified as the July 2002 average from three different sources (Reynolds, RTG and AMSR) and was held constant throughout each model integration.

For each configuration, the WRF model was spun up for 2 days from the beginning of July 2002 and the surface wind field averaged over the subsequent 28 days of model integration was compared with the QuikSCAT and ECMWF wind speed fields averaged over the same 28-day period. The 28-day WRF, QuikSCAT and ECMWF wind speed fields were spatially high-pass filtered with half-power filter cutoffs of 30º of longitude by 10º of latitude to isolate the SST influence on surface winds. The WRF model

simulations were then assessed by comparing the coupling coefficient for wind speed response to SST deduced from each model run with the coupling coefficients derived from QuikSCAT observations and the ECMWF model. The influence of SST on low-level winds was also assessed from the wavenumber power spectral density (PSD) of wind speed, which decomposes the spatial variance of wind speed as a function of wavenumber or, equivalently, wavelength.

3.1. Sensitivity to the SST Boundary Condition, Horizontal Mixing and Model Grid Resolution

The accuracy of model representations of the observed air-sea interaction depends critically on the accuracy and resolution of the SST boundary condition. The coarse ~900 km zonal by ~600 km meridional smoothing inherent in the Reynolds SST analyses (Reynolds et al., 2002) that were used prior to 9 May 2001 in the ECMWF model severely limits the accuracy of the surface wind response to SST. The importance of the SST boundary condition is shown in Fig. 3 from WRF simulations with three different SST boundary conditions (Reynolds, RTG and AMSR), but with otherwise identical model configurations. The surface wind fields are highly correlated spatially with whichever SST field is used as the boundary condition. The presence or absence of small-scale structure in the WRF surface wind field in the top panels of Fig. 3 is therefore dependent on the presence or absence of small-scale structure in the SST field. This is also evident from the direct correspondence between the wavenumber spectra of SST and wind speed for the three model runs (bottom two panels of Fig. 3).

The coupling coefficients from spatially high-pass filtered monthly averages of the WRF simulations differ only slightly for the three SST boundary conditions (right panels of Fig. 3); a given change in SST thus produces essentially the same wind speed response, regardless of the detailed accuracy and resolution of the SST field that is used for the ocean surface boundary condition. The coupling coefficient is therefore a robust measure of the low-level wind response to SST, and hence of the ability of the model to represent the air-sea interaction phenomenon that is of interest here.

While the spatial structures of the small-scale variability in the ECMWF surface wind fields forced with the RTG SST analyses are in good agreement with QuikSCAT observations (left panels of Figs. 1a and b), their intensity is visually too small by about a factor of two, consistent with the approximate factor-of-two underestimation of the coupling coefficients (right panels of Figs. 1a and b; see also Maloney and Chelton, 2006). Resolution limitations of the RTG SST analyses affect the accuracy of surface winds in WRF model simulations only on wavelength scales shorter than about 250 km (see the wavenumber spectra of wind speed in the bottom right panel of Fig. 3; see also Song et al. 2008), which is the approximate resolution of the RTG SST analyses (Thiebaux et al., 2003; Chelton and Wentz, 2005; see also the wavenumber spectra of SST in the bottom left panel of Fig. 3).

Horizontal mixing in the WRF model is similarly a limiting factor only on wavelength scales shorter than about 250 km (see the left panel of Fig. 6 below). Moreover, the WRF simulations also show that the ~40 km grid resolution of the TL511 spectral dynamical core used in the ECMWF operational model from 21 November 2000 to 31 January 2006 is a limiting factor only on scales shorter than about 250 km (see again the left panel of Fig. 6 below). Song et al. (2008) thus concluded that the approximate factor-of-2 underestimation of variance of surface winds in the ECMWF model on wavelength scales of 250–1000 km is due primarily to inadequacies in the parameterization of vertical turbulent mixing.

It is clear from Fig. 1c and analogous figures for the other coupled climate models analyzed by Maloney and Chelton (2006) that grid resolution becomes a more limiting factor when it is too coarse. The feature resolution in numerical models is generally a factor of 5 or more coarser than the grid spacing of the model (Walters, 2000). The 100–1000 km scales of SST-induced perturbations of the surface wind field are

therefore not adequately resolved by coupled climate models that typically have grid spacings of 1.4° or coarser that cannot resolve features smaller than about 7°.

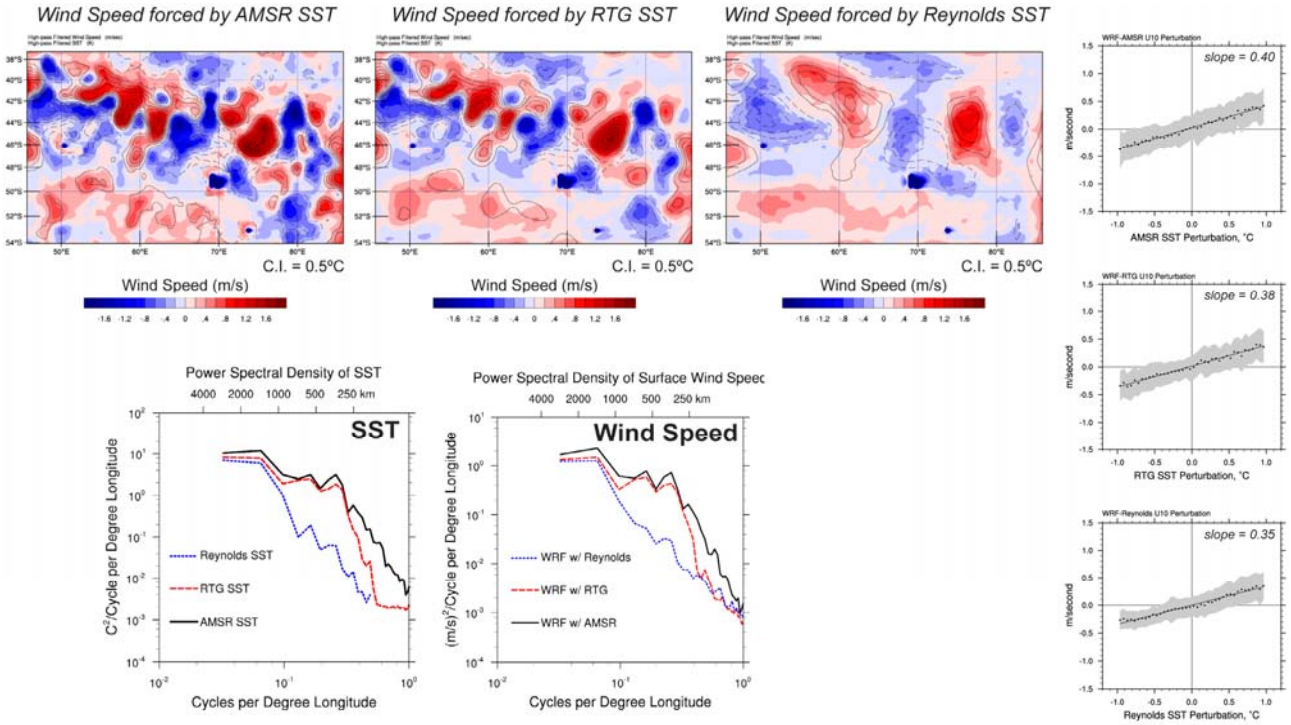

Figure 3 Monthly average maps and zonal wavenumber spectra of SST and 10-m wind speed from the WRF mesoscale model with three different SST boundary conditions (AMSR satellite observations, the RTG SST analyses, and the Reynolds SST analyses) for July 2002, forced at the outer boundaries by the NCEP operational model. The SST boundary condition was held constant over each model integration. Spatially high-pass filtered wind speed and SST are shown in the top panels as color and contours, respectively, with a contour interval of 0.5°C. Binned scatter plots of 10-m wind speed as functions of SST are shown in the right panels for each model run. (After Song et al., 2008.)

3.2. Sensitivity to Vertical Mixing

As noted above, the resolution limitation of the RTG SST boundary condition, the model grid resolution and horizontal mixing all affect the WRF model results only on scales shorter than about 250 km over the ranges of model characteristics relevant to the ECMWF model. It is therefore hypothesized that the underestimation of variance in the ECMWF model (see Figs. 1a and b) is attributable to inadequacies in the parameterization of vertical mixing.

The sensitivity of surface wind speed to vertical mixing was investigated by Song et al. (2008) from the WRF model by parameterizing the vertical eddy diffusivity in the Mellor and Yamada (1982) form as

$$K_m = Q_m \, l \, e^{1/2},$$

where e is the turbulent kinetic energy (TKE), l is a turbulent length scale and Q_m is a stability function defined to have the form

$$Q_m = S_m^N + R_s \, (5S_m - S_m^N).$$

Here S_m is the Mellor and Yamada (1982) stability function and S_m^N is its value in neutrally stable conditions. The stability response factor R_s modulates the dependence of vertical diffusion on stability. A value of R_s=1 corresponds to the stability function $Q_m = 5S_m$ that Grenier and Bretherton (2001) found resulted in vertical profiles of TKE that matched the profiles obtained from a large-eddy (LES) simulation model. Values of R_s<1 correspond to reduced sensitivity of vertical mixing to stability, which is manifest as stronger mixing in stable conditions and weaker mixing in unstable conditions compared with the mixing obtained when R_s=1.

The WRF model with R_s=1 yields a monthly average u_{10}^N field very similar to the QuikSCAT observations (left panels of Fig. 4) with coupling coefficient essentially identical to that derived from the QuikSCAT observations (right panels of Fig. 4). The wavenumber spectral characteristics of the resulting WRF model simulation of u_{10}^N are also very similar to the QuikSCAT observations (Song et al., 2008).

To assess the sensitivity of surface wind speed to vertical mixing, the WRF model was run with R_s values ranging from 0.1 to 1.1 in increments of 0.1, and with 40 km grid spacing and RTG SST boundary condition that mimic the ECMWF model formulation for the time period 9 May 2001 through 31 January 2006. The model run with R_s=0.3 yields a monthly average u_{10} field very similar to that from the ECMWF model (left panels of Fig. 5) with coupling coefficient essential identical to that derived from the ECMWF model (right panels of Fig. 5). The PSD of u_{10} from the WRF model runs with R_s=0.2 and 0.4 bracket the PSD computed from u_{10} in the ECMWF analyses (left panel of Fig. 6). These results suggest that the vertical mixing in the ECMWF model is comparable to that in the WRF model with R_s≈0.3. This value of R_s is very similar to the Mellor and Yamada (1982) mixing (thin solid line in the left panel of Fig. 6).

For comparison, the PSD of the monthly average u_{10} field in the WRF simulation with R_s=1.0 is shown for 40 km grid spacing by the green line in the left panel of Fig. 6. On wavelengths longer than ~250 km, the variance is more than a factor of 2 greater than in the simulations with R_s=0.2 and 0.4, as well as with the Mellor-Yamada formulation of mixing. Improving the grid spacing to 25 km and less dissipative horizontal diffusion only affect the PSD at wavelengths shorter than ~250 km (red line in the left panel of Fig. 6).

The coupling coefficients derived from the WRF model simulations over the full range of stability response factors R_s considered by Song et al. (2008) are shown in the right panel of Fig. 6. It can be seen that the value of R_s=0.3 used for the WRF simulation in the bottom panel of Fig. 5 yields a coupling coefficient for u_{10} that

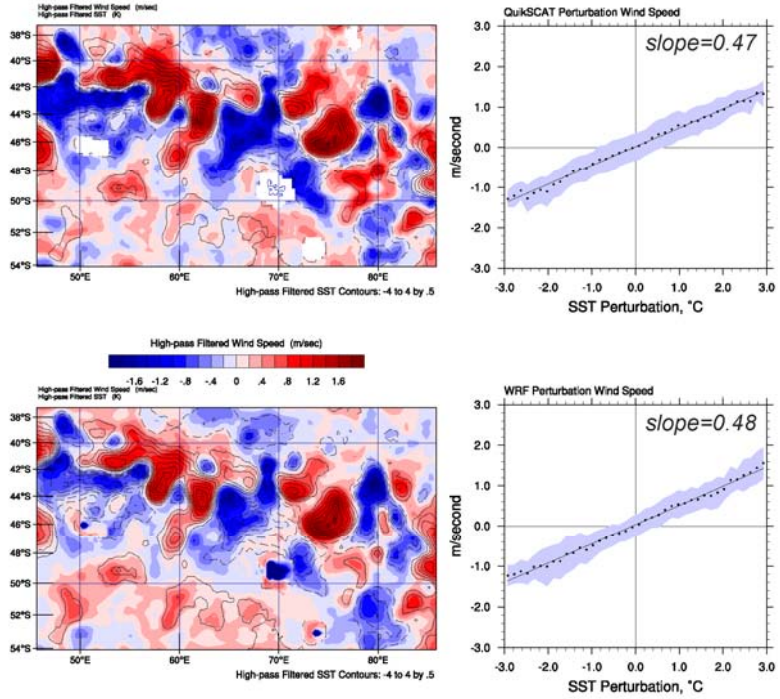

Figure 4 Monthly averages of 10-m equivalent neutral stability wind speed from (top) QuikSCAT observations and (bottom) the WRF model with 25-km grid spacing, 6th-order horizontal diffusion filter, and with response factor R_s=1.0 (see text) for vertical mixing. The model was forced at the outer boundaries by the NCEP operational model and the SST boundary condition was specified as the July 2002 monthly average AMSR satellite SST. The SST boundary condition was held constant over the full model integration. Spatially high-pass filtered wind speed and SST are shown in the left panels as color and contours, respectively, with a contour interval of 0.5°C. Binned scatter plots of wind speed as a function of SST are shown in the right panels. (After Song et al., 2008.)

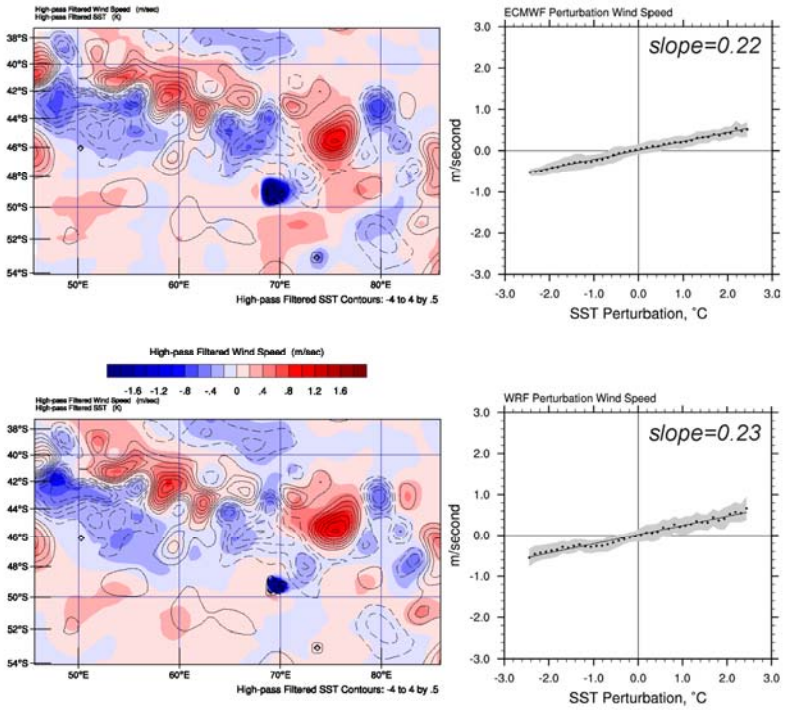

Figure 5 The same as Fig. 4, except 10-m wind speed from (top) the ECMWF operational model and (bottom) the WRF model with 40-km grid spacing, 4th-order horizontal diffusion filter, and with response factor R_s=0.3 (see text) for vertical mixing. The model was forced at the outer boundaries by the NCEP operational model and the SST boundary condition was specified as the July 2002 monthly average RTG SST. The SST boundary condition was held constant over the full model integration. (After Song et al., 2008.)

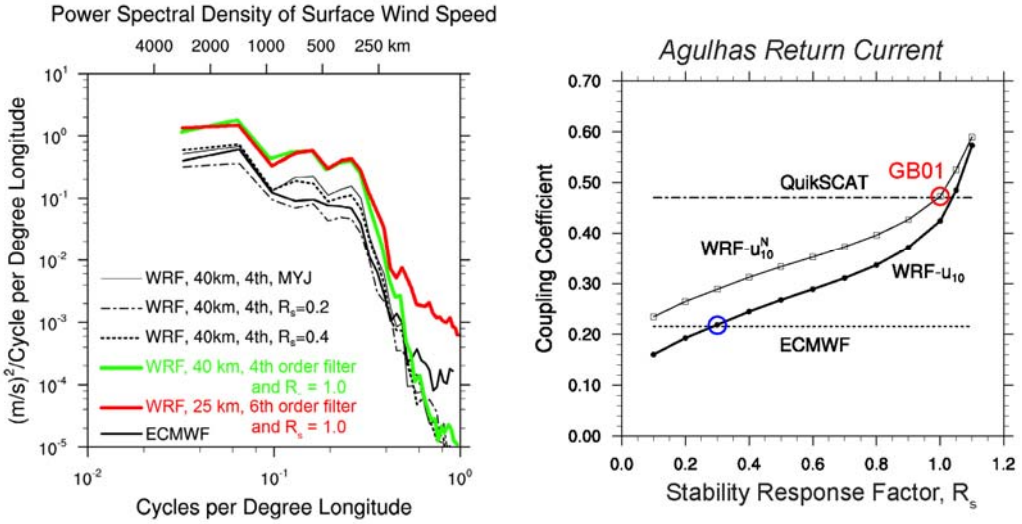

Figure 6 Left: Along-track wavenumber spectra from the operational ECMWF model (thick solid black line) and five different runs of the WRF model with SST boundary condition specified by the July 2002 monthly average RTG SST, and forced at the outer boundaries by the NCEP operational model. Except for the red line, all of the spectra from the WRF model are based on 40 km grid spacing and a 4th-order horizontal diffusion filter. The red line is based on 25 km grid spacing and a 6th-order horizontal diffusion filter. The green and red lines are from model runs with the Grenier and Bretherton (2001) parameterization of vertical mixing (R_s=1.0); the more dissipative 4th-order horizontal diffusion and the coarser 40 km grid spacing both damp the kinetic energy only on wavelengths shorter than about 250 km. Right: The coupling coefficients (the slopes of straight-line fits of binned averages of wind speed as a function of SST) for 12 different runs of the WRF model with 40-km grid spacing, a 4th-order horizontal diffusion filter, RTG SST boundary condition, and varying dependence of vertical mixing on atmospheric boundary layer stability, parameterized by the response factor R_s. The coupling coefficients are shown both in terms of 10-m wind speed (solid circles) and the 10-m equivalent neutral stability wind speed (open squares). The coupling coefficients determined from the QuikSCAT observations and the operational ECMWF model are shown by horizontal lines. (After Song et al., 2008.)

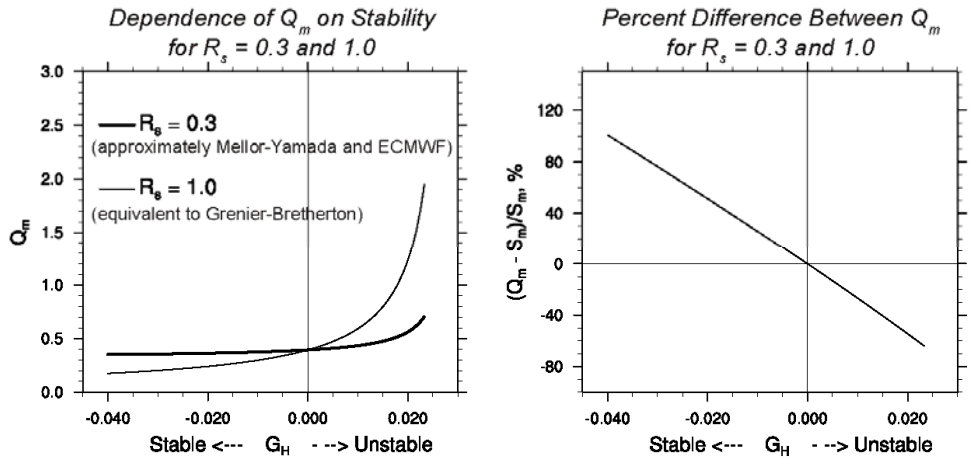

Figure 7 Left: The dependence of the stability function Q_m on the stability parameter G_H (see Mellor and Yamada, 1982) for stability response factors of R_s=0.3 (heavy solid line) and 1.0 (thin solid line). Right: The percentage difference between the values of Q_m for R_s=0.3 and 1.0 in the left panel. (From Song et al., 2008.)

most closely matches that derived from the ECMWF model. The value of R_s=1.0 used for the WRF simulation in the bottom panel of Fig. 4 yields a coupling coefficient for u_{10}^N that most closely matches that derived from the QuikSCAT observations. This provides an entirely independent confirmation of the conclusion of Grenier and Bretherton (2001) that R_s=1.0 yields WRF model wind fields that are in closest agreement with observations. The dependence of the Mellor-Yamada mixing on atmospheric stability is thus too weak by the multiplicative factor of 5 in the Grenier-Bretherton formulation.

The results of Figs. 5 and 6 suggest that the underestimation of variance in the ECMWF model on scales smaller than ~1000 km is likely due to the model having a vertical mixing parameterization that is comparable to the WRF simulation with R_s=0.3, approximately equivalent to the Mellor-Yamada form of mixing parameterization. The implications of this form of mixing compared with the Grenier and Bretherton (2001) formulation with R_s=1.0 are evident from Fig. 7, which shows the dependencies of vertical mixing on stability for R_s=0.3 and 1.0.

4. Conclusions

The observational evidence that SST exerts a strong influence on surface winds is unequivocal. Winds are locally stronger over warmer water and weaker over cooler water. Spatial variations in the SST field thus result in spatial variations in the surface wind field, resulting in wind stress curl structures that generate open-ocean upwelling and drive the large-scale ocean circulation. The magnitudes of these SST-induced wind stress curl anomalies are order-1 perturbations of the large-scale wind stress curl (Chelton et al., 2004). This ocean-atmosphere interaction thus likely has important feedback effects on the ocean circulation, as well as on air-sea heat fluxes and ocean biology. It is therefore crucial that this SST influence on surface winds be accurately represented in the wind fields that are used to force ocean circulation models. Most ocean models are forced by the surface wind analyses or reanalyses from the ECMWF or NCEP models. As shown in Figs. 1, 4 and 5, these models underestimate the SST influence on surface winds by a factor of 2 or more. Likewise, this ocean-atmosphere coupling is underestimated by a factor of 2 or more in coupled climate models (Fig. 1c; see also Maloney and Chelton, 2006).

Evidence has recently been presented that the SST influence on the atmosphere on the scales of 100–1000 km considered in this study penetrates into the troposphere. Surface convergence and divergence associated with spatial variations in the SST field (Chelton et al., 2004) generate vertical motion in the Gulf Stream

region that is clearly evident throughout the troposphere (Minobe et al., 2008). SST influence has also been detected throughout the troposphere in the Agulhas Return Current region (Liu et al., 2007). The ocean-atmosphere interaction identified from the satellite observations may therefore be important to the general circulation of the atmosphere, again emphasizing the importance of accurate representation of the SST influence on surface winds in operational forecast models and coupled climate models.

The conclusions from the WRF simulations summarized here are that the primary factors responsible for underestimation of SST-induced small-scale variability in the surface wind field are: 1) model grid resolution; 2) the resolution of the SST boundary condition in uncoupled models (and presumably the resolution of the ocean component of coupled models); and 3) parameterization of vertical mixing sensitivity to atmospheric stability. Ongoing studies with the ECMWF model and the U.K. Met Office model indicate that it is a major challenge to increase the vertical mixing sensitivity to stability by the amount required to match the coupling between SST and surface wind speed deduced from the satellite observations without introducing adverse effects on other aspects of the model simulations.

In the case of the ECMWF model, we conclude that is is likely that the approximate factor-of-2 underestimation of the surface wind response to SST is attributable primarily to underestimation of the dependence of vertical mixing on atmospheric stability. The resolution of the SST boundary condition is a secondary issue in the ECMWF model, but is the most limiting factor in the NCEP model that presently continues to use the Reynolds SST analyses as the ocean boundary condition. The resolution of the ocean component of coupled models is presumably important for the same reason that the resolution of the SST boundary condition is important for operational forecast models.

For coupled climate models, the representation of SST influence on surface winds depends also on the grid resolution. While the observed SST influence is adequately resolved on scales longer than about 250 km by the grid resolutions of present operational forecast models, the grid resolutions of many coupled models are too coarse to represent this ocean-atmosphere interaction accurately.

References

Chelton, D. B., 2005: The impact of SST specification on ECMWF surface wind stress fields in the eastern tropical Pacific. *J. Climate*, **18**, 530-550.

Chelton, D. B., and M. H. Freilich, 2005: Scatterometer-based assessment of 10-m wind analyses from the operational ECMWF and NCEP numerical weather prediction models. *Mon. Wea. Rev.*, **133**, 409-429

Chelton, D. B., and F. J. Wentz, 2005: Global microwave satellite observations of sea-surface temperature for numerical weather prediction and climate research. *Bull. Amer. Meteor. Soc.*, **86**, 1097-1115.

Chelton, D. B., M. G. Schlax, M. H. Freilich, and R. F. Milliff, 2004: Satellite measurements reveal persistent small-scale features in ocean winds. *Science*, **303**, 978-983.

Grenier, H., and C. S. Bretherton, 2001: A moist PBL parameterization for large-scale models and its application to subtropical cloud-topped marine boundary layers. *Mon. Wea. Rev.*, **129**, 357-377.

Liu, W. T. and W. Tang, 1996: Equivalent neutral wind. JPL Publication 96-17, Pasadena, CA, 8 pp.

Liu, W. T., X. Xie, and P. Niiler, 2007: Ocean-atmosphere interaction over Agulhas Extension meanders. *J. Clim.*, **20**, 5784—5797.

Maloney, E. D., and D. B. Chelton, 2006: An assessment of the sea surface temperature influence on surface wind stress in numerical weather prediction and climate models. *J. Climate*, **19**, 2743-2762.

Mears, C. A., D. K. Smith and F. J. Wentz, 2001: Comparison of Special Sensor Microwave Imager and buoy-measured wind speeds from 1987 to 1997. *J. Geophys. Res.*, **106**, 11,719-11,729.

Mellor, G. and T. Yamada, 1982: Development of a turbulent closure model for geophysical fluid problems. *Rev. Astrophys. Space Phys.*, **20**, 851-875.

Minobe, S., A. Kuwano-Yoshida, N. Komori, S.-P. Xie, and R. J. Small, 2008: Influence of the Gulf Stream on the troposphere. *Nature*, **452**, 206-209.

O'Neill, L. W., D. B. Chelton, S. K. Esbensen, and N. Thum, 2008: The effects of SST-induced horizontal wind speed and direction gradients on mid-latitude vorticity and divergence fields: observations and numerical simulation. *J. Clim.*, submitted.

Reynolds, R. W., N. A. Rayner, T. M. Smith, D. C. Stokes, and W. Wang, 2002: An improved in situ and satellite SST analysis for climate. *J. Climate*, **15**, 1609-1625.

Small, R. J., and Coauthors, 2008: Air-sea interaction over ocean fronts and eddies. *Dyn. Atmos. Oceans*, doi:10.1016/j.dynatmoce.2008.01.001.

Song, Q., D. B. Chelton, S. K. Esbensen, N. Thum, and L. W. O'Neill, 2008: Coupling between sea surface temperature and low-level winds in mesoscale numerical models. *J. Clim.*, in press.

Thiébaux, J., E. Rogers, W. Wang, and B. Katz, 2003: A new high-resolution blended real-time global sea surface temperature analysis. *Bull. Amer. Meteor. Soc.*, **84**, 645-656.

Walters, M. K., 2000: Comments on "The differentiation between grid spacing and resolution and their application to numerical modeling". *Bull. Amer. Meteor. Soc.*, **81**, 2475-2477.

Xie, S.-P., 2004: Satellite observations of cool ocean-atmosphere interaction. *Bull. Amer. Meteorol. Soc.*, **85**, 195-208.